Critical behaviors of lattice $U(1)$ gauge models and three-dimensional Abelian-Higgs gauge field theory

Claudio Bonati,[1] Andrea Pelissetto,[2] and Ettore Vicari[1]
[1]*Dipartimento di Fisica dell'Università di Pisa and INFN Largo Pontecorvo 3, I-56127 Pisa, Italy*
[2]*Dipartimento di Fisica dell'Università di Roma Sapienza and INFN Sezione di Roma I, I-00185 Roma, Italy*

(Received 11 January 2022; revised 2 February 2022; accepted 2 February 2022; published 7 February 2022)

We investigate under which conditions the three-dimensional (3D) multicomponent Abelian-Higgs (AH) field theory (scalar electrodynamics) is the continuum limit of statistical lattice gauge models, i.e., when it characterizes the universal behavior at critical transitions occurring in these models. We perform Monte Carlo simulations of the lattice AH model with compact gauge fields and N-component scalar fields with charge $q \geqslant 2$ for $N = 15$ and 25. Finite-size scaling analyses of the Monte Carlo data show that the transitions along the line separating the confined and deconfined phases are continuous and that they belong to the same universality class for any $q \geqslant 2$. Moreover, they are in the same universality class as the transitions in the lattice AH model with noncompact gauge fields along the Coulomb-to-Higgs transition line. We finally argue that these critical behaviors are described by the stable charged fixed point of the renormalization-group flow of the 3D AH field theory.

DOI: 10.1103/PhysRevB.105.085112

I. INTRODUCTION

Three-dimensional (3D) Abelian $U(1)$ gauge models with multicomponent scalar fields and SU(N) global symmetry ($N \geqslant 2$)—the Abelian-Higgs (AH) models—emerge in many physical situations. They provide effective theories for superconductors, superfluids, and quantum SU(N) antiferromagnets [1–8]. In particular, they are expected to describe the transition between the Néel and the valence-bond-solid state in two-dimensional antiferromagnetic SU(2) quantum systems [9–16], which represents the paradigmatic model for the so-called deconfined quantum criticality [17]. In this context several studies have focused on systems with two scalar components [7,9–37].

Classical and quantum Abelian models have been extensively studied with the purpose of identifying their phases and the nature of their phase transitions. It has been realized that a crucial role is played by topological aspects, like Berry phases, monopoles, or the compact/noncompact nature of the $U(1)$ gauge fields, together with the charge of the scalar fields. Indeed, the phase diagram and the nature of the transitions is different in lattice AH models with compact and noncompact gauge fields [18,38], in AH compact models with charge-one and higher-charge scalar fields [18,39], and in models with or without topological defects such as monopoles [19–21,40].

Multicomponent lattice AH models with $U(1)$ gauge invariance and SU(N) global symmetry are the lattice counterparts of the multicomponent scalar electrodynamics or AH field theory, in which an N-component complex scalar field $\boldsymbol{\Phi}(\boldsymbol{x})$ is minimally coupled to the electromagnetic field $A_\mu(\boldsymbol{x})$. The corresponding continuum Lagrangian reads

$$\mathcal{L} = |D_\mu \boldsymbol{\Phi}|^2 + r\, \boldsymbol{\Phi}^* \boldsymbol{\Phi} + \frac{1}{6} u\, (\boldsymbol{\Phi}^* \boldsymbol{\Phi})^2 + \frac{1}{4g^2} F_{\mu\nu}^2, \qquad (1)$$

where $F_{\mu\nu} \equiv \partial_\mu A_\nu - \partial_\nu A_\mu$ and $D_\mu \equiv \partial_\mu + i A_\mu$. Its renormalization-group (RG) flow was investigated perturbatively, using the $\varepsilon \equiv 4 - d$ expansion [41–45], in the functional RG [46] and in the large-N approach [41,47–50]. These studies showed that a stable charged fixed point (CFP) with a nonzero gauge coupling exists only when the number N of components is larger than N_D^*, where N_D^* depends on the space dimension D. Close to four dimensions, a stable CFP exists only in systems with a very large number of components, since $N_4^* = 90 + 24\sqrt{15} \approx 183$. However, N_D^* drastically decreases in three dimensions, $N_3^* \ll N_4^*$. The 3D value N_3^* has been estimated by constrained resummations of the four-loop ε expansion using two-dimensional results [43], obtaining $N_3^* = 12(4)$, and from the analysis of Monte Carlo results for the noncompact lattice AH model [38], obtaining $N_3^* = 7(2)$.

On general grounds, one would expect the stable CFP of the 3D RG flow of the AH field theory to be associated with the universality class of critical transitions in 3D systems with local $U(1)$ and global SU(N) symmetry. However, the behavior of lattice AH models is not so simple. Indeed, they present different phases and transitions belonging to different universality classes, depending on features that are not present in the continuum field theory. At present we do not yet satisfactorily understand under which conditions statistical models have transitions controlled by the field-theory CFP. In particular, it is not clear which are the key features of those lattice $U(1)$ gauge models that have critical transitions described by the field-theory CFP of the RG flow of the AH field theory.

In general, critical transitions in lattice gauge theories can be classified into two different groups:

(i) Transitions in which only matter correlations are critical; at the transition gauge variables do not display long-range correlations.

(ii) Transitions in which matter and gauge-field correlations are both critical.

In case (i), although gauge variables are not critical, the gauge symmetry is crucial for identifying the scalar critical degrees of freedom. Indeed, gauge symmetry prevents nongauge invariant correlators from acquiring nonvanishing vacuum expectation values and developing long-range order: the gauge symmetry hinders some scalar degrees of freedom—those that are not gauge invariant—from becoming critical. In this case the critical behavior or continuum limit is driven by the condensation of gauge-invariant scalar operators, which play the role of fundamental fields in the Landau-Ginzburg-Wilson (LGW) theory that provides an effective description of the critical regime, without including the gauge fields. The lattice CP^{N-1} model is an example of a $U(1)$ gauge model that shows this type of behavior [40,51]. Two-dimensional $U(1)$ gauge models with multicomponent scalar matter [52] and several lattice non-Abelian gauge Higgs models in two and three dimensions [53–59] also belong to class (i).

In case (ii), in which both scalar and gauge correlations are critical at the transition, an appropriate effective field-theory description of the critical behavior requires explicit gauge fields. Therefore, one would expect that the field-theory CFP of the RG flow of the AH field theory is the one that controls the universal features of the critical transitions of type (ii) in AH lattice models. Critical behaviors consistent with the universality classes of the AH field theory have been observed in the lattice AH model with noncompact gauge fields [38] (along the transition line that separates the Coulomb and the Higgs phase), and in the lattice AH model with compact gauge fields and $q = 2$ scalar charge [39] (along the transition line between the confined and the deconfined phase). We also mention that continuous transitions of type (ii) have been observed in a different lattice $U(1)$ gauge model, in the CP^{N-1} model without monopoles [21]. However, they do not belong to the same universality class as those observed in the noncompact lattice AH model [38].

In this paper we return to this issue, strengthening previous results. We provide compelling numerical evidence that, for a sufficiently large number of components N, $N \gtrsim 10$, say, the continuous transitions between the confined and deconfined phase of the lattice AH model with compact gauge fields and scalar charge $q \geqslant 2$ belong to the same universality class for any $q \geqslant 2$. Moreover, the critical behavior is the same as in the noncompact AH model, which is formally obtained in the limit $q \to \infty$. A detailed finite-size scaling (FSS) analysis of the Monte Carlo (MC) results allows us to obtain precise estimates of the critical exponents. They turn out to be in excellent agreement with the field-theory predictions, obtained in the large-N expansion [41,48,49]. Therefore, we conclude that the CFP of the AH field theory is associated with a line of critical transitions that is present in the lattice AH model with compact gauge fields and any scalar charge $q \geqslant 2$ and in the model with noncompact gauge fields. In all cases, the field-theory critical behavior (or continuum limit) is observed along the transition line that occurs in the small gauge-coupling part of the phase diagram.

The paper is organized as follows. In Sec. II we define the compact and the noncompact lattice AH model and summarize the main features of their phase diagram. In Sec. III we define the observables used in the numerical simulations and present the results of the numerical analyses. Finally, in Sec. IV we draw our conclusions.

II. COMPACT AND NONCOMPACT FORMULATIONS OF LATTICE AH MODELS

In this section we define the compact and noncompact formulations of the multicomponent lattice AH model on a cubic lattice, and summarize the known results for their phase diagrams. In both formulations the scalar fields are unit-length N-component complex variables $\boldsymbol{z}_{\boldsymbol{x}}$ associated with the lattice sites. The gauge fields are either complex phases $\lambda_{\boldsymbol{x},\mu}$ (compact model) or real numbers $A_{\boldsymbol{x},\mu}$ (noncompact model) associated with the lattice links.

A. AH model with compact gauge variables

In the compact formulation we define a gauge variable $\lambda_{\boldsymbol{x},\mu} \in U(1)$ ($|\lambda_{\boldsymbol{x},\mu}| = 1$) on each lattice link (it starts at site $\boldsymbol{x}$ along one of the lattice direction, $\mu = 1, 2, 3$). The compact AH model with N-component scalar fields of integer charge q is defined by the partition function

$$Z = \sum_{\{z,\lambda\}} e^{-\beta H_c}, \tag{2}$$

where the Hamiltonian reads

$$H_c = -JN \sum_{\boldsymbol{x},\mu} 2\,\mathrm{Re}\big(\bar{\boldsymbol{z}}_{\boldsymbol{x}} \cdot \lambda^q_{\boldsymbol{x},\mu}\, \boldsymbol{z}_{\boldsymbol{x}+\hat{\mu}}\big) - \kappa \sum_{\boldsymbol{x},\mu>\nu} 2\,\mathrm{Re}\,(\lambda_{\boldsymbol{x},\mu}\, \lambda_{\boldsymbol{x}+\hat{\mu},\nu}\, \bar{\lambda}_{\boldsymbol{x}+\hat{\nu},\mu}\, \bar{\lambda}_{\boldsymbol{x},\nu}). \tag{3}$$

Here the two sums run over all lattice links and plaquettes, respectively. In the following we rescale J and κ by β, thus formally setting $\beta = 1$. The parameter $\kappa \geqslant 0$ plays the role of inverse gauge coupling.

The compact AH model presents a disordered (confined) phase for small values of J and one (for $q = 1$) or two (for $q \geqslant 2$) low-temperature ordered phases for large values of J. The transitions between the disordered and the ordered phases are associated with the breaking of the global SU(N) symmetry. The corresponding order parameter is the gauge-invariant bilinear operator

$$Q^{ab}_{\boldsymbol{x}} = \bar{z}^a_{\boldsymbol{x}} z^b_{\boldsymbol{x}} - \frac{1}{N}\delta^{ab}. \tag{4}$$

For $\kappa = 0$ the model is equivalent to a particular lattice formulation of the CP^{N-1} model, which undergoes a phase transition at a finite value of J (see, e.g., Ref. [40]). In the $\kappa \to \infty$ limit the model reduces to an $O(2N)$ vector model, which presents a transition at a finite value of J, as well.

For $q = 1$, only two phases are present, see Fig. 1 (top): A disordered phase for small J and an ordered phase for large J. They are separated by a single transition line, along which only gauge-invariant scalar modes become critical. Gauge fields do not develop long-range correlations, but they prevent

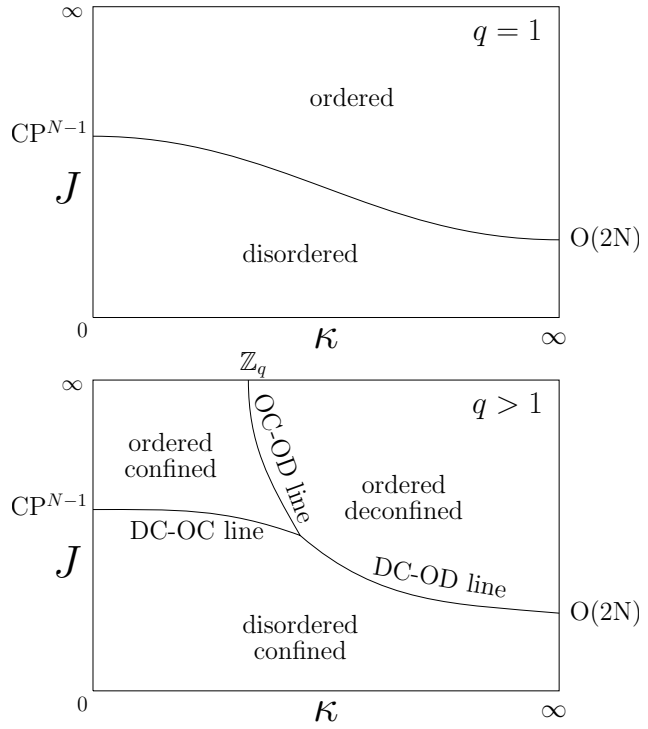

FIG. 1. Sketch of the phase diagram of the 3D compact lattice AH model, in which a compact $U(1)$ gauge field is coupled to an N-component unit-length complex scalar field with charge q, for generic $N \geqslant 2$. In the upper panel we report the phase diagram for $q = 1$, with two phases separated by a single transition line. In the lower panel we report the phase diagram for $q = 2$, with three phases, the disordered-confined (DC), the ordered-deconfined (OD), and the ordered-confined (OC) phases. The AH model is equivalent to the CP^{N-1} model for $\kappa = 0$, to the $O(2N)$ vector model for $\kappa \to \infty$. For $J \to \infty$ and $q \geqslant 2$, we obtain the lattice $\mathbb{Z}_q$ gauge model.

gauge-dependent scalar correlations, such as the vector correlations $\langle \bar{z}_{\boldsymbol{x}} \cdot z_{\boldsymbol{y}} \rangle$, from becoming critical. As a consequence, the critical behavior is described by a LGW Φ^4 theory in terms of a gauge-invariant scalar order parameter. The fundamental field is a traceless Hermitian matrix field $\Psi^{ab}(\boldsymbol{x})$, which can be formally defined by coarse graining the lattice order parameter $Q^{ab}_{\boldsymbol{x}}$, defined in Eq. (4). The LGW field theory is obtained by considering the most general fourth-order polynomial in Ψ consistent with the $U(N)$ global symmetry [40,60]:

$$\mathcal{L}_{\rm LGW} = \mathrm{Tr}(\partial_\mu \Psi)^2 + r\,\mathrm{Tr}\,\Psi^2 + w\,\mathrm{tr}\,\Psi^3 + u\,(\mathrm{Tr}\,\Psi^2)^2 + v\,\mathrm{Tr}\,\Psi^4. \quad (5)$$

In this approach, continuous transitions are possible only if the RG flow in the LGW theory has a stable fixed point. For $N = 2$ the Lagrangian (5) is equivalent to that of the $O(3)$ vector model (in particular, the Ψ^3 term cancels), thus continuous transitions in the Heisenberg universality class [61] can be observed in the $N = 2$ AH model. For larger values of N, the LGW approach predicts all transitions to be of first order, because of the presence of the Ψ^3 term [18,40,51].

For $q \geqslant 2$ the phase diagram is more complex, see Fig. 1 (bottom), with three different phases [39,62–68]. They are characterized by the large-distance behavior of both scalar and gauge observables. Beside the scalar gauge-invariant observable (4), one may consider the Wilson loop of the gauge fields that signals the confinement or deconfinement of charge-one external static sources. As shown in Fig. 1, for small J and any $\kappa \geqslant 0$, there is a phase in which scalar-field correlations are disordered and single-charge particles are confined (the Wilson loop obeys the area law). For large values of J (low-temperature region) scalar correlations are ordered and the $SU(N)$ symmetry is broken. Two different phases occur here: For small κ, single-charge particles are confined, while they are deconfined for large κ.

The three different phases are separated by three transition lines meeting at a multicritical point: The DC-OD transition line between the disordered-confined (DC) and the ordered-deconfined (OD) phases, the DC-OC line between the disordered-confined and ordered-confined (OC) phases, and the OC-OD line between the ordered-confined and ordered-deconfined phases. The transition lines have different features, since they are associated with different phases. Moreover, their nature depends on the number N of components and on the charge q of the scalar matter. The transitions along the DC-OC line are the same as that in the 3D CP^{N-1} model for $\kappa = 0$. They are continuous for $N = 2$, belonging to the $O(3)$ vector universality class, and of first order for $N \geqslant 3$. For $J = \infty$, the model (3) is equivalent to a $\mathbb{Z}_q$ gauge model [39]. A natural hypothesis is that the transitions along the OC-OD line belong to the universality class of the $\mathbb{Z}_q$ gauge model. This hypothesis has been verified numerically for $q = 2$ [39], for which $\kappa_c = 0.380706646(6)$ in the limit $J \to \infty$. Finally, transitions along the DC-OD line are continuous for large values of N, as we shall see below, and belong to the same universality class for any $q \geqslant 2$. We shall argue that they realize the continuum limit of the AH field theory (1).

B. AH model with noncompact gauge variables

In the noncompact formulation the fundamental gauge variable is the real vector field $A_{\boldsymbol{x},\mu}$. The lattice Hamiltonian reads

$$H_{\rm nc} = -JN \sum_{\boldsymbol{x},\mu} 2\,\mathrm{Re}\,(\bar{z}_{\boldsymbol{x}} \cdot e^{iA_{\boldsymbol{x},\mu}} z_{\boldsymbol{x}+\hat{\mu}}) + \frac{\kappa_g}{2} \sum_{\boldsymbol{x},\mu>\nu} (\Delta_{\hat{\mu}} A_{\boldsymbol{x},\nu} - \Delta_{\hat{\nu}} A_{\boldsymbol{x},\mu})^2, \quad (6)$$

where the sums run over all links and plaquettes, respectively, $\Delta_{\hat{\mu}} A_{\boldsymbol{x}} \equiv A_{\boldsymbol{x}+\hat{\mu}} - A_{\boldsymbol{x}}$, and $\kappa_g \geqslant 0$ corresponds to the inverse gauge coupling $1/g^2$ of the continuum theory (1). The partition function reads

$$Z_{\rm nc} = \sum_{\{z,A\}} e^{-H_{\rm nc}}. \quad (7)$$

Unlike the compact case, the charge q of the scalar field is irrelevant: We can set $q = 1$ by a redefinition of the gauge field $A_{\boldsymbol{x}}$.

At variance with the compact case, the partition function (7) is only formally defined. Since the integration domain for the gauge variables is noncompact, gauge invariance implies $Z_{\rm nc} = \infty$ even on a finite lattice. If periodic boundary conditions are used, this problem is present even when a maximal gauge fixing is added. Indeed, the partition function still diverges because of the presence of gauge-invariant zero modes:

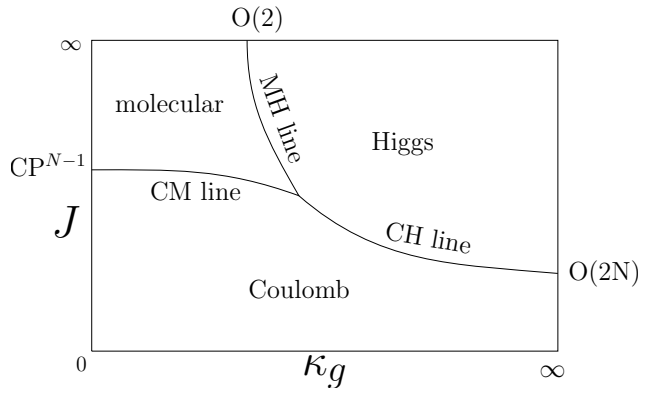

FIG. 2. Sketch of the phase diagram of the lattice AH model with noncompact gauge fields and unit-length N-component complex scalar fields, for generic $N \geqslant 2$. There are three different phases, the Coulomb, Higgs, and molecular phases, and three transition lines: The Coulomb-to-Higgs (CH) line between the Coulomb and Higgs phases, the Coulomb-to-molecular (CM) line, and the molecular-to-Higgs (MH) line. The model is equivalent to the CP^{N-1} model for $\kappa_g = 0$, to the $O(2N)$ vector model for $\kappa_g \to \infty$, and to the inverted XY model for $J \to \infty$.

noncompact gauge-invariant Polyakov operators, i.e., sums of the fields $A_{\boldsymbol{x},\mu}$ along nontrivial paths winding around the lattice [38], are still unbounded. To overcome this problem, C^* boundary conditions [69,70] were considered in Ref. [38]. These boundary conditions preserve gauge invariance and provide a rigorous definition of the partition function in a finite volume.

In Fig. 2 we sketch the phase diagram of the noncompact lattice AH model. For any $N \geqslant 2$ the phase diagram is characterized by three phases. For small J we have a Coulomb phase, in which the global SU(N) symmetry is unbroken and electromagnetic correlations are long ranged. For large J, there are two phases characterized by the breaking of the SU(N) symmetry. They are distinguished by the behavior of the gauge modes. In the Higgs phase (large κ), electromagnetic correlations are gapped, while in the molecular phase (small κ) the electromagnetic field is ungapped.

The Coulomb, molecular, and Higgs phases are separated by three different transition lines meeting at a multicritical point: the CM line between the Coulomb and molecular phases, the MH line between the molecular and Higgs phases, and the CH line between the Coulomb and Higgs phases. Their nature crucially depends on the number N of components. The transitions along the CM line are the same as that in the 3D CP^{N-1} model ($\kappa_g = 0$): they are continuous for $N = 2$, belonging to the $O(3)$ vector universality class, and of first order for $N \geqslant 3$. The transitions along the MH line are expected to be continuous, and to belong to the XY universality class, at least for sufficiently large values of the parameter J [the transition point in the limit $J \to \infty$ is located at $\kappa_{gc} = 0.076051(2)$, obtained by using the estimate $\beta_c = 3.00239(6)$ reported in Ref. [71] and identifying $\kappa_c = \beta_c/(4\pi^2)$]. Finally, transitions along the CH line are continuous for a sufficiently large number N of components. As argued in Ref. [38], they should realize the continuum limit of the AH field theory (1).

C. Relation between the compact and the noncompact model

It is interesting to note that the compact formulation is equivalent to the noncompact one for $q \to \infty$. Indeed, if we rewrite the compact field $\lambda_{\boldsymbol{x},\mu}$ as

$$\lambda_{\boldsymbol{x},\mu} = e^{iA_{\boldsymbol{x},\mu}/q}, \tag{8}$$

with $A_{\boldsymbol{x},\mu} \in [-\pi q, \pi q]$, the Hamiltonian (3) becomes

$$H_c = -JN \sum_{\boldsymbol{x},\mu} 2\,\mathrm{Re}\,(\bar{z}_{\boldsymbol{x}} \cdot e^{iA_{\boldsymbol{x},\mu}}\, z_{\boldsymbol{x}+\hat{\mu}}) - 2\kappa \sum_{\boldsymbol{x},\mu>\nu} \mathrm{Re}\,\exp\left[-\frac{i}{q}(\Delta_{\hat{\mu}} A_{\boldsymbol{x},\nu} - \Delta_{\hat{\nu}} A_{\boldsymbol{x},\mu})\right]. \tag{9}$$

For $q \to \infty$, the gauge fields $A_{\boldsymbol{x},\mu}$ become unbounded and the Hamiltonian is equivalent to that of the noncompact formulation, provided that $\kappa_g = 2\kappa/q^2$. Note that the equivalence trivially holds as long as the fluctuations of $A_{\boldsymbol{x},\mu}$ on each plaquette are bounded and uncorrelated for $q \to \infty$, i.e., for any point of the phase diagram except possibly at phase transitions. Therefore, the noncompact formulation (7) should be recovered from the compact formulation (3) in the limit $q \to \infty$, keeping $\kappa_g = 2\kappa/q^2$ fixed.

The equivalence of the models also holds for $J \to \infty$. In this limit the compact formulation reduces to the $\mathbb{Z}_q$ model

$$H_q = -\kappa^{(q)} \sum_{\boldsymbol{x},\mu>\nu} \mathrm{Re}\,(\lambda_{\boldsymbol{x},\mu}\, \lambda_{\boldsymbol{x}+\hat{\mu},\nu}\, \bar{\lambda}_{\boldsymbol{x}+\hat{\nu},\mu}\, \bar{\lambda}_{\boldsymbol{x},\nu}), \tag{10}$$

where $\kappa^{(q)} = 2\kappa$ and the gauge field takes the values $\lambda_{\boldsymbol{x},\mu} = e^{i\frac{2\pi}{q}n}$, with $n \in 0, 1, \ldots, q-1$. If the limit $q \to \infty$ is smooth, the critical value of the coupling $\kappa^{(q)}$ should scale as

$$\kappa_c^{(q)} \simeq \kappa_{gc}\, q^2 \tag{11}$$

for large q, where $\kappa_{gc} = 0.076051(2)$ is the critical coupling of the inverted XY model that represents the $J \to \infty$ limit of the noncompact model [71]. The q dependence of $\kappa_c^{(q)}$ has been numerically investigated in Refs. [72,73]. Reference [73] determined the large-q behavior, obtaining

$$\kappa_c^{(q)} \simeq C q^2, \tag{12}$$

with $C = 0.076053(4)$ [we use the estimate $A = 1.50122(7)$ reported in Ref. [73], identifying $C = A/(2\pi^2)$], which is in excellent agreement with the estimate of κ_{gc}.

The argument presented above only proves that the compact model converges to the noncompact one as $q \to \infty$, but does not provide us with any information on the critical behavior. For the $\mathbb{Z}_q$ transition observed for $J \to \infty$, numerical results [73] indicate that the transition belongs to the XY universality class for any $q \geqslant 5$. Thus, for these values of q, the compact $\mathbb{Z}_q$ model and the noncompact inverted XY model have a transition in the same universality class. In the next section we will present numerical results showing that the same occurs at the transitions controlled by the CFP of the AH field theory. For N large enough and any $q \geqslant 2$, the transitions along the CH line of the noncompact model and along the DC-OD line of the compact model belong to the same universality class, controlled by the CFP.

III. NUMERICAL ANALYSES

We have performed MC simulations of the compact AH model with $N = 15$ and $N = 25$ and some values of $q \geqslant 2$. We use C^* boundary conditions, as we did for the noncompact model [38]. This allows us to compare the FSS results—universal scaling curves depend on boundary conditions—for the compact model with those for the noncompact one. The results of the FSS analyses of the MC data will provide strong evidence that, for any $q \geqslant 2$, the continuous transitions along the DC-OD transition line, running up to $\kappa \to \infty$, belong to the same universality class as those along the CH transition line of the noncompact formulation.

We will also compute the correlation-length exponent ν and the exponent η_q that characterizes the singular behavior of the susceptibility of the bilinear field Q_x. The results will be compared with the large-N predictions [41,48]

$$\nu = 1 - \frac{48}{\pi^2 N} + O(N^{-2}), \tag{13}$$

$$\eta_q = 1 - \frac{32}{\pi^2 N} + O(N^{-2}). \tag{14}$$

The good agreement of the numerical estimates of the critical exponents with the large-N field-theory expressions demonstrates that these continuous transitions are associated with the CFP of the AH field theory (1).

A. Observables and finite-size scaling

To characterize phase transitions associated with the breaking of the SU(N) symmetry, we consider correlations of the gauge-invariant bilinear operator Q defined in Eq. (4). Since Q is periodic when using C^* boundary conditions, its two-point correlation function can be defined as

$$G(\boldsymbol{x} - \boldsymbol{y}) = \langle \mathrm{Tr}\, Q_{\boldsymbol{x}} Q_{\boldsymbol{y}} \rangle. \tag{15}$$

The corresponding susceptibility and correlation length are defined as $\chi = \sum_{\boldsymbol{x}} G(\boldsymbol{x})$ and

$$\xi^2 \equiv \frac{1}{4 \sin^2(\pi/L)} \frac{\widetilde{G}(\boldsymbol{0}) - \widetilde{G}(\boldsymbol{p}_m)}{\widetilde{G}(\boldsymbol{p}_m)}, \tag{16}$$

where $\widetilde{G}(\boldsymbol{p}) = \sum_{\boldsymbol{x}} e^{i\boldsymbol{p}\cdot\boldsymbol{x}} G(\boldsymbol{x})$ is the Fourier transform of $G(\boldsymbol{x})$, and $\boldsymbol{p}_m = (2\pi/L, 0, 0)$.

In our analysis we consider RG invariant quantities, such as $R_\xi = \xi/L$ and the Binder parameter

$$U = \frac{\langle \mu_2^2 \rangle}{\langle \mu_2 \rangle^2}, \quad \mu_2 = \sum_{\boldsymbol{x},\boldsymbol{y}} \mathrm{Tr}\, Q_{\boldsymbol{x}} Q_{\boldsymbol{y}}. \tag{17}$$

At a continuous phase transition, any RG invariant ratio R scales as [61]

$$R(j, L) = f_R(X) + L^{-\omega} g_R(X) + \cdots, \tag{18}$$

where

$$X = (j - j_c) L^{1/\nu}. \tag{19}$$

Here ν is the correlation-length critical exponent, ω is the leading correction-to-scaling exponent, j is the Hamiltonian parameter driving the transition, and j_c is the critical point (we will perform simulations varying J at fixed κ or κ_g for the compact and noncompact model, respectively, so that j should be identified with J). The function $f_R(X)$ is universal up to a multiplicative rescaling of its argument. Assuming that R_ξ is a monotonically increasing function of j, we can combine the RG predictions for U and R_ξ to obtain

$$U(j, L) = F(R_\xi) + O(L^{-\omega}), \tag{20}$$

where F depends only on the universality class, boundary conditions, and lattice shape, without nonuniversal factors. Equation (20) is particularly convenient because it allows us to test universality-class predictions without requiring a tuning of nonuniversal parameters.

The exponent ν will be determined from the FSS behavior of R_ξ and U, assuming the scaling behavior (18). The exponent η_q will be computed from the scaling behavior of the susceptibility χ. In the FSS limit, it scales as

$$\chi(j, L) = L^{2-\eta_q} [f_\chi(X) + L^{-\omega} g_\chi(X) + \cdots], \tag{21}$$

where X is defined in Eq. (19).

B. Monte Carlo results

Let us first report our results for $N = 25$. We have considered two values of q, $q = 2$ and 3, and, for each of them, we have performed simulations at a fixed value of κ, chosen so that the transition belongs to the DC-OD line. For $q = 2$, simulations were already performed [39] fixing $\kappa = 1$ and using periodic boundary conditions, identifying the transition at $J_c = 0.29333(3)$. For $q = 3$, the results of Ref. [73] indicate that the OC-OD line ends at $\kappa_c = 0.5422(1)$ for $J \to \infty$. To be on the safe side, we have performed simulation keeping $\kappa = 2$ fixed, observing a transition for $J = J_c \approx 0.2945$.

To verify whether the transitions for $q = 2$ and $q = 3$ belong to the same universality class as the transitions in the noncompact model along the CH line, in Fig. 3 we report the Binder parameter U versus the ratio R_ξ. The compact-model data fall on top of the curve obtained from simulations of the noncompact model [38]. The agreement is excellent for both values of q. These results demonstrate that the continuous transitions in the compact model (DC-OD line) and in the noncompact model (CH line) all belong to the same universality class.

For $q = 2$ we also estimated the critical exponents, performing the same analysis we did in Refs. [38,39]. To estimate the exponent ν, we perform combined fits of U and R_ξ to Eq. (18). We parametrize the scaling functions $f_R(X)$ and $g_R(X)$ with polynomials (we use 24th-order and 8th-order polynomials for the two functions, respectively). We perform fits including only data with $L \geqslant 16$, varying the exponent ω in the range [0.6,1.2] (results depend marginally on the value of this exponent). We only consider data in the interval $X \in [X_{\min}, X_{\max}]$, varying $X_{\min}$ (between -0.5 and -0.3) and $X_{\max}$ (between 0.15 and 0.25). Results are stable. We obtain $J_c = 0.293331(2)$ (in excellent agreement with the estimate of Ref. [39] reported above) and

$$\nu = 0.817(7). \tag{22}$$

The error includes the statistical error and also takes into account the variation of the estimate as the fit parameters are changed.

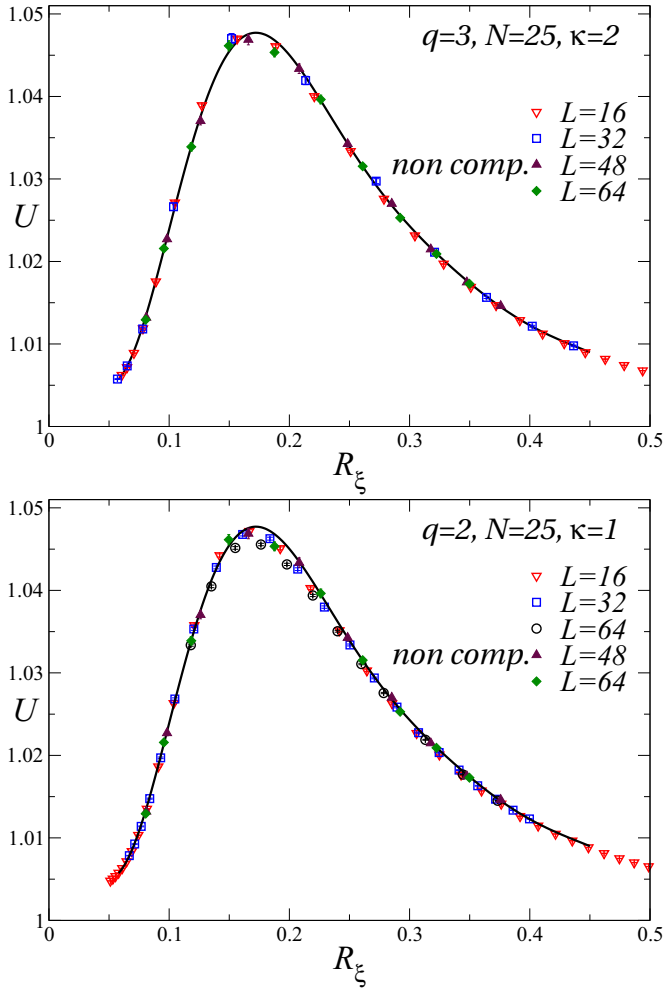

FIG. 3. Estimates of U versus R_ξ for the compact AH model with $N = 25$ and C^* boundary conditions. Top: Results for $q = 3$, $\kappa = 2$; bottom: results for $q = 2$, $\kappa = 1$. The continuous line in each panel is an extrapolation of data for the noncompact AH model [38]; noncompact-model data for $L = 48$ and $L = 64$ are also reported to provide an estimate of the accuracy of the extrapolation.

To estimate η_q we have performed fits to

$$\ln \chi = (2 - \eta_q) \ln L + h_{1\chi}(X) + L^{-\omega} h_{2\chi}(X), \tag{23}$$

parametrizing $h_{1\chi}(X)$ and $h_{2\chi}(X)$ with polynomials. In this case fits are sensitive to the value of ω. We end up with $\omega = 1.05(10)$ and

$$\eta_q = 0.882(2). \tag{24}$$

The estimates (22) and (24) are significantly more accurate than, but consistent with, previous determinations. Reference [38] obtained $\nu = 0.802(8)$ for the compact model with $q = 2$, while Ref. [39] reported $\nu = 0.815(15)$ for the noncompact model. As for η_q, previous estimates are $\eta_q = 0.88(2)$ (compact model with $q = 2$), and $\eta_q = 0.883(7)$ (noncompact model).

We have performed a similar analysis for $N = 15$. In this case we have considered $q = 2$, $q = 3$, and $q = 4$, performing simulations at fixed κ along the DC-OD line. For $q = 2$ and $q = 3$ we have performed simulations at $\kappa = 1$ (transition at $J \approx 0.307$) and at $\kappa = 2$ (transition at $J \approx 0.308$), respectively, as we did for $N = 25$. For $q = 4$ we have chosen $\kappa = 4$. Given that the OC-OD line ends at [72,73] $\kappa = 0.76135(2)$, $J = \infty$, this choice should guarantee that the transition we observe for $J \approx 0.304$ belongs to the DC-OD line.

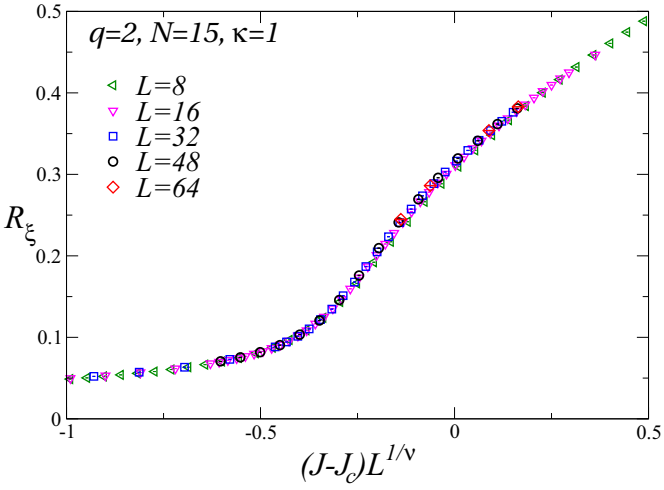

FIG. 4. FSS plot of R_ξ for $q = 2$ and $N = 15$ at $\kappa = 1$, obtained by using the values $J_c = 0.306957$ and $\nu = 0.728$ for the critical coupling and the critical exponent, respectively.

To compute the critical exponents in the $N = 15$ case we consider only the data with $q = 2$, since scaling corrections appear to be smaller than for $q = 4$ and only a limited number of lattice sizes is available $q = 3$. The combined analysis of the Binder parameter and of R_ξ gives $J_c = 0.306957(4)$ and

$$\nu = 0.728(5), \tag{25}$$

which is in agreement with the noncompact-model estimate $\nu = 0.721(3)$, obtained in Ref. [38]. The excellent quality of the scaling obtained in this way is shown in Fig. 4. Again the error on ν takes into account statistical errors and how the estimate changes as the fit parameters are varied. In particular, the quoted result is consistent with an exponent ω varying between 0.6 and 1. We also estimate the exponent η_q, obtaining

$$\eta_q = 0.815(3), \tag{26}$$

which is in full agreement with the estimate 0.815(10), obtained in the noncompact model [38].

The results for the Binder parameter as a function of R_ξ are reported in Fig. 5 for $q = 2$ and $q = 3$. Once again, data for the noncompact lattice AH model with $N = 15$ (from Ref. [38]) are also shown for comparison. In this case scaling corrections are larger than for $N = 25$. To provide further evidence that the data approach the universal curve computed in the noncompact model, in the inset of Fig. 5 we report the deviations from the universal curve rescaled with L^ω. We use $\omega = 1$ in the plot, but values in the range $0.6 \leqslant \omega \leqslant 1$, as suggested by the fits, give qualitatively similar plots. Results fall approximately on the same curve that has the same qualitative features both for $q = 2$ and $q = 3$, as expected on the basis of universality. Results for $q = 4$ are shown in Fig. 6. In this case, corrections to scaling are large and, in spite of the large lattices considered—we performed simulations up to $L = 64$—the compact-model data are not yet close to

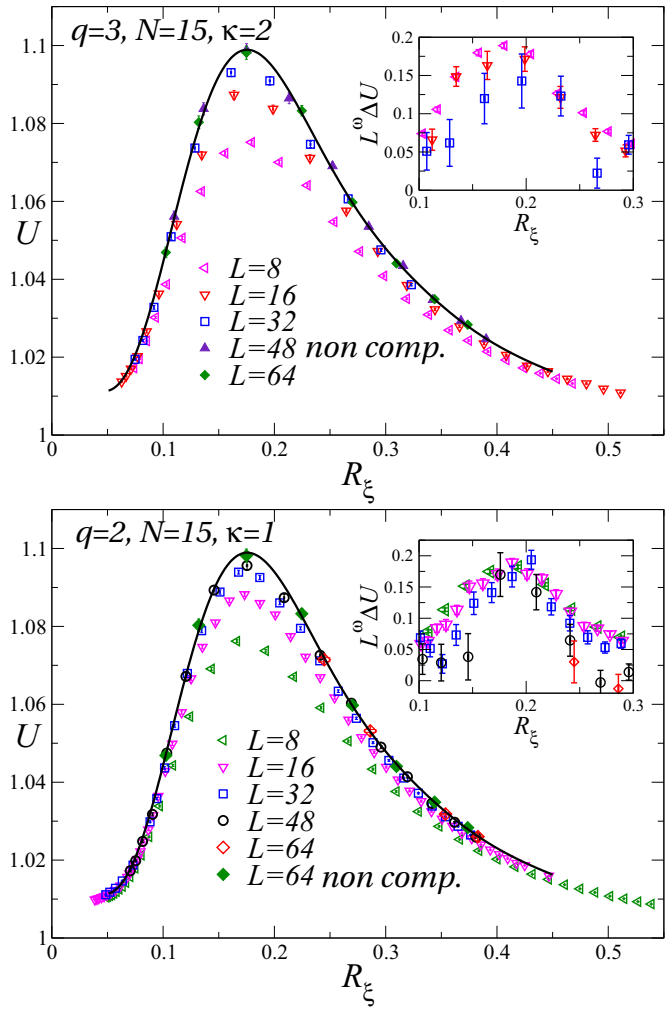

FIG. 5. Estimates of U versus R_ξ for the compact AH model with $N = 15$ and C^* boundary conditions. Top: Results for $q = 3$ and $\kappa = 2$, bottom: results for $q = 2$ and $\kappa = 1$; The continuous line is an extrapolation of the data for the noncompact model [38]; noncompact-model data for $L = 48$ and $L = 64$ are also reported to provide an estimate of the accuracy of the extrapolation. The insets show the deviations from the extrapolated results: we report $L^\omega \Delta U$, where for each data point $\Delta U = U - f_U(R_\xi)$ and $f_U(R_\xi)$ is the extrapolation of the data for the noncompact model (continuous line in the main panels). We set $\omega = 1$, but little changes if we decrease ω as far as $\omega \gtrsim 0.6$.

the noncompact-model curve, although they show the correct trend as L increases. Most probably, this is a crossover effect due to the $O(2N)$ fixed point that controls the critical behavior for $\kappa = \infty$. Indeed, its presence gives rise to crossover effects that increase with κ and that can become particularly strong for the simulations that have been performed along the line with $\kappa = 4$.

C. Comparison with the large-N computations

The estimates of the critical exponents for $N = 15$ and 25 are displayed in Fig. 7, together with the leading-order large-N estimates Eqs. (13) and (14). They would predict $\nu = 0.805$, $\eta_q = 0.870$ for $N = 25$ and $\nu = 0.676$, $\eta_q = 0.784$

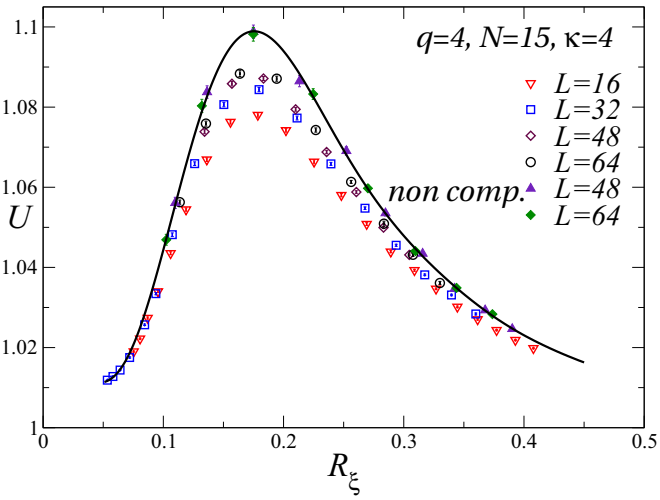

FIG. 6. Estimates of U versus R_ξ for the compact AH model with $N = 15$ and C^* boundary conditions. Results for $q = 4$ and $\kappa = 4$. The continuous line is an extrapolation of the data for the noncompact model [38]; noncompact-model data for $L = 48$ and $L = 64$ are also reported to provide an estimate of the accuracy of the extrapolation.

for $N = 15$, to be compared with the previously obtained numerical results $\nu = 0.817(7)$, $\eta_q = 0.882(2)$ for $N = 25$ [see Eqs. (22) and (24)], and $\nu = 0.728(5)$, $\eta_q = 0.815(3)$ for $N = 15$ [see Eqs. (25) and (26)]. The values of the critical exponents for $N = 25$ are very close to their leading-order large-N estimates, and deviations from the $O(N^{-1})$ asymptotic behavior are consistent with a next-to-leading $O(N^{-2})$ correction. If we assume

$$\nu = 1 - \frac{48}{\pi^2 N} + \frac{a_\nu}{N^2},$$
$$\eta_q = 1 - \frac{32}{\pi^2 N} + \frac{a_\eta}{N^2}. \tag{27}$$

and we fix the unknown parameters by requiring these expressions to be exact for $N = 25$, we obtain the estimates $a_\nu = 7(4)$ and $a_\eta = 7(1)$. Using these values, we would predict $\nu = 0.708(19)$ and $\eta_q = 0.816(6)$ for $N = 15$, in agreement with the estimates (25) and (26). For $N = 10$ we would predict $\nu = 0.59(4)$ and $\eta_q = 0.749(13)$, again in substantial agreement with the results $\nu = 0.64(2)$, $\eta_q = 0.74(2)$ of Ref. [38] for the noncompact model. By fitting to Eq. (27) all the results for ν and η_q obtained in this work, in the noncompact model [38], and in compact model with periodic boundary conditions (only $q = 2$, $N = 25$) [39] we obtain

$$a_\nu = 10.5(5), \quad a_\eta = 7.0(5), \tag{28}$$

and the results of this phenomenological interpolation are shown in Fig. 7.

IV. CONCLUSIONS

We have investigated whether and under which conditions the 3D multicomponent AH field theory (scalar electrodynamics) is realized as the continuum limit of statistical lattice

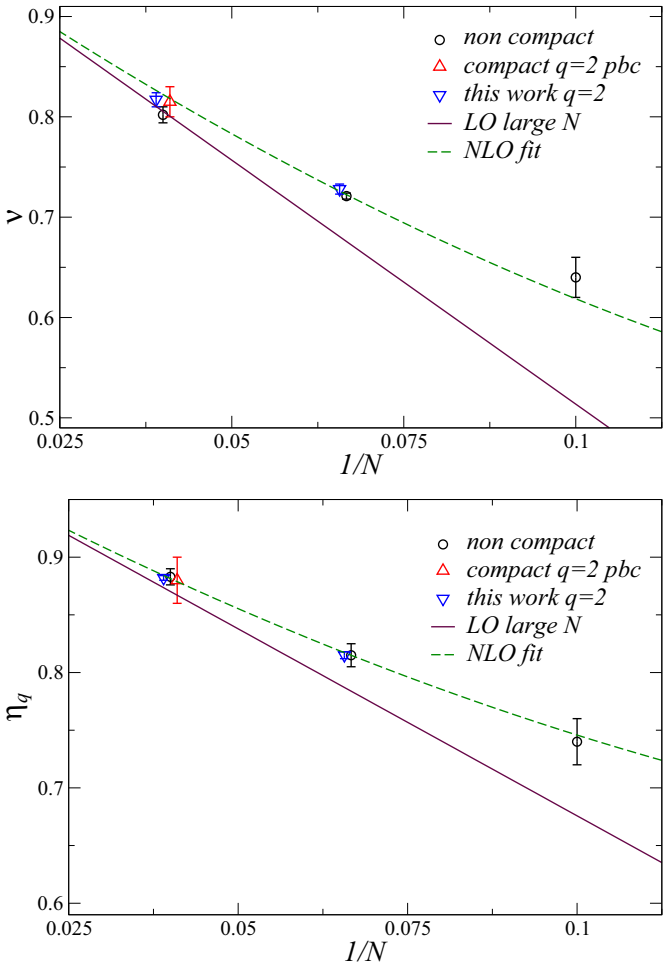

FIG. 7. Critical exponents ν (top) and η_q (bottom) versus $1/N$. We report: results ($N = 10, 15, 25$) for the noncompact model [38]; results ($N = 25$ only) for the compact model with $q = 2$ and periodic boundary conditions (pbc) [39]; the results for $N = 15$ and 25 of the present work ($q = 2$); the leading-order (LO) large-N predictions [Eqs. (13) and (14)]; the phenomenological next-to-leading (NLO) interpolations, Eq. (27) with $a_\nu = 10.5$, $a_\eta = 7.0$.

gauge models. For this purpose we consider a lattice model with unit-length degenerate N-component scalar fields of charge q coupled to compact gauge fields with $U(1)$ local and SU(N) global invariance.

The FSS analyses of the MC results show that, for $q \geqslant 2$, the transitions along the line that separates the confined and deconfined phases, see Fig. 1 (bottom), are continuous for a sufficiently large number of components (we perform a detailed study for $N = 15$ and 25) and that they belong to the same universality class for any $q \geqslant 2$. Moreover, they are in the same universality class as the transitions along the CH line (see Fig. 2), in the lattice AH model with noncompact gauge fields. Since both scalar and gauge correlations are critical along the CH line, the effective field-theory description of these transitions is provided by the AH field theory with Lagrangian (1), with explicit gauge fields. The stable CFP point of the RG flow of the AH field theory, which is present for $N \geqslant N_3^*$ with $N_3^* = 7(2)$, should characterize the universal features of these transition lines (the OC-OD line in the compact model with $q \geqslant 2$, see Fig. 1 (bottom), and the CH line in the noncompact model, see Fig. 2).

We believe that these results improve our understanding of the critical behavior (continuum limit) of gauge field theories in dimension lower than four, which are relevant in condensed-matter physics, see, e.g., Refs. [74–76]. In particular, they shed light on the conditions under which we may expect to observe transitions controlled by the CFP of the RG flow of 3D gauge field theories. This issue is also relevant for non-Abelian gauge theories with matter fields; see, e.g., Refs. [54,55,77,78] for related discussions. We believe that further investigations are called for, to achieve a satisfactory understanding of the nonperturbative regimes of Abelian and non-Abelian gauge field theories.

ACKNOWLEDGMENTS

Numerical simulations have been performed using the Green Data Center of the University of Pisa.

[1] N. Read and S. Sachdev, Spin-Peierls, valence-bond solid, and Néel ground states of low-dimensional quantum antiferromagnets, Phys. Rev. B **42**, 4568 (1990).

[2] S. Takashima, I. Ichinose, and T. Matsui, $CP^1 + U(1)$ lattice gauge theory in three dimensions: Phase structure, spins, gauge bosons, and instantons, Phys. Rev. B **72**, 075112 (2005).

[3] S. Takashima, I. Ichinose, and T. Matsui, Deconfinement of spinons on critical points: Multiflavor $CP^1 + U(1)$ lattice gauge theory in three dimension, Phys. Rev. B **73**, 075119 (2006).

[4] R. K. Kaul, Quantum phase transitions in bilayer SU(N) antiferromagnets, Phys. Rev. B **85**, 180411(R) (2012).

[5] R. K. Kaul and A. W. Sandvik, Lattice Model for the SU(N) Néel to Valence-Bond Solid Quantum Phase Transition at Large N, Phys. Rev. Lett. **108**, 137201 (2012).

[6] M. S. Block, R. G. Melko, and R. K. Kaul, Fate of CP^{N-1} Fixed Point with q Monopoles, Phys. Rev. Lett. **111**, 137202 (2013).

[7] A. Nahum, J. T. Chalker, P. Serna, M. Ortuño, and A. M. Somoza, Deconfined Quantum Criticality, Scaling Violations, and Classical Loop Models, Phys. Rev. X **5**, 041048 (2015).

[8] C. Wang, A. Nahum, M. A. Metliski, C. Xu, and T. Senthil, Deconfined Quantum Critical Points: Symmetries and Dualities, Phys. Rev. X **7**, 031051 (2017).

[9] A. W. Sandvik, Evidence for Deconfined Quantum Criticality in a Two-Dimensional Heisenberg Model with Four-Spin Interactions, Phys. Rev. Lett. **98**, 227202 (2007).

[10] R. G. Melko and R. K. Kaul, Scaling in the Fan of an Unconventional Quantum Critical Point, Phys. Rev. Lett. **100**, 017203 (2008).

[11] F. J. Jiang, M. Nyfeler, S. Chandrasekharan, and U. J. Wiese, From an antiferromagnet to a valence bond solid: Evidence for a first-order phase transition, J. Stat. Mech. (2008) P02009.

[12] A. W. Sandvik, Continuous Quantum Phase Transition between an Antiferromagnet and a Valence-Bond Solid in Two Dimensions: Evidence for Logarithmic Corrections to Scaling, Phys. Rev. Lett. **104**, 177201 (2010).

[13] K. Harada, T. Suzuki, T. Okubo, H. Matsuo, J. Lou, H. Watanabe, S. Todo, and N. Kawashima, Possibility of deconfined criticality in SU(N) Heisenberg models at small N, Phys. Rev. B **88**, 220408(R) (2013).

[14] K. Chen, Y. Huang, Y. Deng, A. B. Kuklov, N. V. Prokof'ev, and B. V. Svistunov, Deconfined Criticality Flow in the Heisenberg Model with Ring-Exchange Interactions, Phys. Rev. Lett. **110**, 185701 (2013).

[15] S. Pujari, K. Damle, and F. Alet, Nèel-State to Valence-Bond-Solid Transition on the Honeycomb Lattice: Evidence for Deconfined Criticality, Phys. Rev. Lett. **111**, 087203 (2013).

[16] H. Shao, W. Guo, and A. W. Sandvik, Quantum criticality with two length scales, Science **352**, 213 (2016).

[17] T. Senthil, L. Balents, S. Sachdev, A. Vishwanath, and M. P. A. Fisher, Quantum criticality beyond the Landau-Ginzburg-Wilson paradigm, Phys. Rev. B **70**, 144407 (2004).

[18] A. Pelissetto and E. Vicari, Multicomponent compact Abelian-Higgs lattice models, Phys. Rev. E **100**, 042134 (2019).

[19] G. Murthy and S. Sachdev, Actions of hedgehogs instantons in the disordered phase of 2+1 dimensional CP^{N-1} model, Nucl. Phys. B **344**, 557 (1990).

[20] O. I. Motrunich and A. Vishwanath, Emergent photons and transitions in the O(3) σ-model with hedgehog suppression, Phys. Rev. B **10**, 075104 (2004).

[21] A. Pelissetto and E. Vicari, Three-dimensional monopole-free CP^{N-1} models, Phys. Rev. E **101**, 062136 (2020).

[22] A. B. Kuklov, N. V. Prokof'ev, B. V. Svistunov, and M. Troyer, Deconfined criticality, runaway flow in the two-component scalar electrodynamics and weak first-order superfluid-solid transitions, Ann. Phys. **321**, 1602 (2006).

[23] O. I. Motrunich and A. Vishwanath, Comparative study of Higgs transition in one-component and two-component lattice superconductor models, arXiv:0805.1494.

[24] A. B. Kuklov, M. Matsumoto, N. V. Prokof'ev, B. V. Svistunov, and M. Troyer, Deconfined Criticality: Generic First-Order Transition in the SU(2) Symmetry Case, Phys. Rev. Lett. **101**, 050405 (2008).

[25] A. B. Kuklov, M. Matsumoto, N. V. Prokof'ev, B. V. Svistunov, and M. Troyer, Comment on "Comparative study of Higgs transition in one-component and two-component lattice superconductor models", arXiv:0805.2578.

[26] D. Charrier, F. Alet, and P. Pujol, Gauge Theory Picture of an Ordering Transition in a Dimer Model, Phys. Rev. Lett. **101**, 167205 (2008).

[27] J. Lou, A. W. Sandvik, and N. Kawashima, Antiferromagnetic to valence-bond-solid transitions in two-dimensional SU(N) Heisenberg models with multispin interactions, Phys. Rev. B **80**, 180414(R) (2009).

[28] G. Chen, J. Gukelberger, S. Trebst, F. Alet, and L. Balents, Coulomb gas transitions in three-dimensional classical dimer models, Phys. Rev. B **80**, 045112 (2009).

[29] D. Charrier and F. Alet, Phase diagram of an extended classical dimer model, Phys. Rev. B **82**, 014429 (2010).

[30] A. Banerjee, K. Damle, and F. Alet, Impurity spin texture at a deconfined quantum critical point, Phys. Rev. B **82**, 155139 (2010).

[31] E. V. Herland, T. A. Bojesen, E. Babaev, and A. Sudbø, Phase structure and phase transitions in a three-dimensional SU(2) superconductor, Phys. Rev. B **87**, 134503 (2013).

[32] L. Bartosch, Corrections to scaling in the critical theory of deconfined criticality, Phys. Rev. B **88**, 195140 (2013).

[33] T. A. Bojesen and A. Sudbø, Berry phases, current lattices, and suppression of phase transitions in a lattice gauge theory of quantum antiferromagnets, Phys. Rev. B **88**, 094412 (2013).

[34] A. Nahum, P. Serna, J. T. Chalker, M. Ortuño, and A. M. Somoza, Emergent SO(5) Symmetry at the Néel to Valence-Bond-Solid Transition, Phys. Rev. Lett. **115**, 267203 (2015).

[35] G. J. Sreejith and S. Powell, Scaling dimensions of higher-charge monopoles at deconfined critical points, Phys. Rev. B **92**, 184413 (2015).

[36] P. Serna and A. Nahum, Emergence and spontaneous breaking of approximate O(4) symmetry at a weakly first-order deconfined phase transition, Phys. Rev. B **99**, 195110 (2019).

[37] A. W. Sandvik and B. Zhao, Consistent scaling exponents at the deconfined quantum-critical point, Chin. Phys. Lett. **37**, 057502 (2020).

[38] C. Bonati, A. Pelissetto, and E. Vicari, Lattice Abelian-Higgs model with noncompact gauge fields, Phys. Rev. B **103**, 085104 (2021).

[39] C. Bonati, A. Pelissetto, and E. Vicari, Higher-charge three-dimensional compact lattice Abelian-Higgs models, Phys. Rev. E **102**, 062151 (2020).

[40] A. Pelissetto and E. Vicari, Three-dimensional ferromagnetic CP^{N-1} models, Phys. Rev. E **100**, 022122 (2019).

[41] B. I. Halperin, T. C. Lubensky, and S. K. Ma, First-Order Phase Transitions in Superconductors and Smectic-A Liquid Crystals, Phys. Rev. Lett. **32**, 292 (1974).

[42] R. Folk and Y. Holovatch, On the critical fluctuations in superconductors, J. Phys. A **29**, 3409 (1996).

[43] B. Ihrig, N. Zerf, P. Marquard, I. F. Herbut, and M. M. Scherer, Abelian Higgs model at four loops, fixed-point collision and deconfined criticality, Phys. Rev. B **100**, 134507 (2019).

[44] K. G. Wilson and J. Kogut, The renormalization group and the ϵ expansion, Phys. Rep. **12**, 77 (1974).

[45] M. E. Fisher, The renormalization group in the theory of critical behavior, Rev. Mod. Phys. **47**, 543 (1975).

[46] G. Fejos and T. Hatsuda, Renormalization group flows of the N-component Abelian Higgs model, Phys. Rev. D **96**, 056018 (2017).

[47] P. Di Vecchia, A. Holtkamp, R. Musto, F. Nicodemi, and R. Pettorino, Lattice CP^{N-1} models and their large-N behaviour, Nucl. Phys. B **190**, 719 (1981).

[48] V. Yu. Irkhin, A. A. Katanin, and M. I. Katsnelson, $1/N$ expansion for critical exponents of magnetic phase transitions in the CP^{N-1} model for $2 < d < 4$, Phys. Rev. B **54**, 11953 (1996).

[49] M. Moshe and J. Zinn-Justin, Quantum field theory in the large N limit: A review, Phys. Rep. **385**, 69 (2003).

[50] R. K. Kaul and S. Sachdev, Quantum criticality of U(1) gauge theories with fermionic and bosonic matter in two spatial dimensions, Phys. Rev. B **77**, 155105 (2008).

[51] A. Pelissetto and E. Vicari, Large-N behavior of three-dimensional lattice CP^{N-1} models, J. Stat. Mech.: Theory Exp. (2020) 033209.

[52] C. Bonati, A. Pelissetto, E. Vicari, Two-dimensional multicomponent Abelian-Higgs lattice models, Phys. Rev. D **101**, 034511 (2020).

[53] C. Bonati, A. Pelissetto, and E. Vicari, Phase Diagram, Symmetry Breaking, and Critical Behavior of Three-Dimensional Lattice Multiflavor Scalar Chromodynamics, Phys. Rev. Lett. **123**, 232002 (2019); Three-dimensional lattice multiflavor scalar chromodynamics: Interplay between global and gauge symmetries, Phys. Rev. D **101**, 034505 (2020).

[54] C. Bonati, A. Franchi, A. Pelissetto, and E. Vicari, Phase diagram and Higgs phases of three-dimensional lattice SU(N_c) gauge theories with multiparameter scalar potentials, Phys. Rev. E **104**, 064111 (2021).

[55] C. Bonati, A. Franchi, A. Pelissetto, and E. Vicari, Three-dimensional lattice SU(N_c) gauge theories with scalar matter in the adjoint representation, Phys. Rev. B **104**, 115166 (2021).

[56] C. Bonati, A. Pelissetto, and E. Vicari, Three-dimensional phase transitions in multiflavor scalar SO(N_c) gauge theories, Phys. Rev. E **101**, 062105 (2020).

[57] C. Bonati, A. Pelissetto, and E. Vicari, Universal low-temperature behavior of two-dimensional lattice scalar chromodynamics, Phys. Rev. D **101**, 054503 (2020).

[58] C. Bonati, A. Franchi, A. Pelissetto, and E. Vicari, Asymptotic low-temperature critical behavior of two-dimensional mulitiflavor lattice SO(N_c) gauge theories, Phys. Rev. D **102**, 034512 (2020).

[59] C. Bonati, A. Franchi, A. Pelissetto, and E. Vicari, Two-dimensional lattice SU(N_c) gauge theories with multiflavor adjoint scalar fields, J. High Energy Phys. **05** (2021) 018.

[60] A. Pelissetto, A. Tripodo, and E. Vicari, Landau-Ginzburg-Wilson approach to critical phenomena in the presence of gauge symmetries, Phys. Rev. D **96**, 034505 (2017).

[61] A. Pelissetto and E. Vicari, Critical phenomena and renormalization group theory, Phys. Rep. **368**, 549 (2002).

[62] E. Fradkin and S. Shenker, Phase diagrams of lattice gauge theories with Higgs fields, Phys. Rev. D **19**, 3682 (1979).

[63] A. Sudbø, E. Smørgrav, J. Smiseth, F. S. Nogueira, and J. Hove, Criticality in the (2+1)-Dimensional Compact Higgs Model and Fractionalized Insulators, Phys. Rev. Lett. **89**, 226403 (2002).

[64] J. Smiseth, E. Smørgrav, F. S. Nogueira, J. Hove, and A. Sudbø, Phase structure of $d = 2 + 1$ compact lattice gauge theories and the transition from Mott insulator to fractionalized insulator, Phys. Rev. B **67**, 205104 (2003).

[65] F. S. Nogueira, J. Smiseth, E. Smørgrav, and A. Sudbø, Compact U(1) gauge theories in $2 + 1$ dimensions and the physics of low dimensional insulating materials, Eur. Phys. J. C **33**, 885 (2004).

[66] M. N. Chernodub, R. Feldmann, E.-M. Ilgenfritz, and A. Schiller, The compact $Q = 2$ Abelian Higgs model in the London limit: Vortex-monopole chains and the photon propagator, Phys. Rev. D **71**, 074502 (2005).

[67] M. N. Chernodub, E.-M. Ilgenfritz, and A. Schiller, Phase structure of an Abelian two-Higgs model and high temperature superconductors, Phys. Rev. B **73**, 100506(R) (2006).

[68] S. Wenzel, E. Bittner, W. Janke, and A. M. J. Schakel, Percolation of vortices in the 3D Abelian lattice Higgs model, Nucl. Phys. B **793**, 344 (2008).

[69] A. S. Kronfeld and U. J. Wiese, SU(N) gauge theories with C periodic boundary conditions. 1. Topological structure, Nucl. Phys. B **357**, 521 (1991).

[70] B. Lucini, A. Patella, A. Ramos, and N. Tantalo, Charged hadrons in local finite-volume QED+QCD with C^* boundary conditions, J. High Energy Phys. **02** (2016) 076.

[71] T. Neuhaus, A. Rajantie, and K. Rummukainen, Numerical study of duality and universality in a frozen superconductor, Phys. Rev. B **67**, 014525 (2003).

[72] G. Bhanot and M. Creutz, The phase diagram of Z(n) and u(1) gauge theories in three-dimensions, Phys. Rev. D **21**, 2892 (1980).

[73] O. Borisenko, V. Chelnokov, G. Cortese, M. Gravina, A. Papa, and I. Surzhikov, Critical behavior of 3D Z(N) lattice gauge theories at zero temperature, Nucl. Phys. B **879**, 80 (2014).

[74] S. Sachdev, Topological order, Emergent gauge fields, and Fermi surface reconstruction, Rep. Prog. Phys. **82**, 014001 (2019).

[75] P. W. Anderson, *Basic Notions of Condensed Matter Physics* (Benjamin/Cummings, Menlo Park, CA, 1984).

[76] X.-G. Wen, *Quantum Field Theory of Many-Body Systems: From the Origin of Sound to an Origin of Light and Electrons* (Oxford University Press, Oxford, 2004).

[77] S. Sachdev, H. D. Scammell, M. S. Scheurer, and G. Tarnopolsky, Gauge theory for the cuprates near optimal doping, Phys. Rev. B **99**, 054516 (2019).

[78] H. D. Scammell, K. Patekar, M. S. Scheurer, and S. Sachdev, Phases of SU(2) gauge theory with multiple adjoint Higgs fields in 2+1 dimensions, Phys. Rev. B **101**, 205124 (2020).